Secondary Organic Aerosol Formation from Camphene Oxidation: Measurements and Modeling

Qi Li[1,2], Jia Jiang[1,2], Isaac Afreh [1,2], Kelley C. Barsanti[1,2], David R. Cocker III[1,2]

[1]Department of Chemical and Environmental Engineering, University of California-Riverside, Riverside, California 92521, United States
[2]The Bourns College of Engineering, Center for Environmental Research and Technology, University of California-Riverside, Riverside, California 92507, United States

Correspondence to: Kelley C. Barsanti (kbarsanti@engr.ucr.edu) and David R. Cocker III (dcocker@engr.ucr.edu)

Abstract. While camphene is one of the dominant monoterpenes measured in biogenic and biomass burning emission samples, oxidation of camphene has not been well-studied in environmental chambers and very little is known about its potential to form secondary organic aerosol (SOA). The lack of chamber-derived SOA data for camphene may lead to significant uncertainties in predictions of SOA from oxidation of monoterpenes using existing parameterizations when camphene is a significant contributor to total monoterpenes. Therefore, to advance the understanding of camphene oxidation and SOA formation, and to improve representation of camphene in air quality models, a series of experiments were performed in the University of California Riverside environmental chamber to explore camphene SOA yields and properties across a range of chemical conditions at atmospherically relevant OH concentrations. The experimental results were compared with modeling simulations obtained using two chemically detailed box models, Statewide Air Pollution Research Center (SAPRC) and Generator for Explicit Chemistry and Kinetics of Organics in the Atmosphere (GECKO-A). SOA parameterizations were derived from the chamber data using both the two-product and volatility basis set (VBS) approaches. Experiments performed with added nitrogen oxides (NO_x) resulted in higher SOA yields (up to 64%) than experiments performed without added NO_x (up to 28%). In addition, camphene SOA yields increased with SOA mass (M_o) at lower mass loadings, but a threshold was reached at higher mass loadings in which the SOA yields no longer increased with M_o. SAPRC modeling of the chamber studies suggested that the higher SOA yields at higher initial NO_x levels were primarily due to higher production of peroxy radicals (RO_2) and the generation of highly oxygenated organic molecules (HOMs) formed through unimolecular RO_2 reactions. SAPRC predicted that in the presence of NO_x, camphene RO_2 reacts with NO and the resultant RO_2 undergo hydrogen (H)-shift isomerization reactions; as has been documented previously, such reactions rapidly add oxygen and lead to products with very low volatility (i.e., HOMs). The end products formed in the presence of NO_x have significantly lower volatilities, and higher O:C ratios, than those formed by initial camphene RO_2 reacting with hydroperoxyl radicals (HO_2) or other RO_2. Moreover, particle densities were found to decrease from 1.47 to 1.30 g cm^{-3} as $[HC]_0/[NO_x]_0$ increased and O:C decreased. The observed differences in SOA yields were largely explained by the gas-phase RO_2 chemistry and the competition between $RO_2 + HO_2$, $RO_2 + NO$, $RO_2 + RO_2$, and RO_2 unimolecular reactions.

1 Introduction

On a global scale, biogenic monoterpene emissions are estimated to contribute 14% of the total reactive volatile organic compounds (VOC) flux (Guenther, 1995). Camphene is an ubiquitous monoterpene emitted from biogenic sources (Geron et al., 2000; Hayward et al., 2001; Ludley et al., 2009; Malekniaet al., 2007; White et al., 2008) and pyrogenic sources (Akagi et al., 2013; Gilman et al., 2015; Hatch et al., 2015). Many studies have reported camphene as a top contributor by mass in measured biogenic and pyrogenic monoterpene emissions (Benelli et al., 2018; Hatch et al., 2019; Komenda, 2002; Mazza & Cottrell, 1999; Moukhtar et al., 2006). For example, in measurements of laboratory and prescribed fires reported by Hatch et al. (2019), camphene was among the top two monoterpenes emitted from subalpine and Douglas fir fires based on emission factors (mass of compound emitted/mass of fuel burned).

When emitted to the atmosphere, monoterpenes form oxygenated compounds through reactions with trace oxidants such as hydroxyl radicals (OH), ozone (O_3) and nitrate radicals (NO_3); compounds with sufficiently low volatility can then condense to form secondary organic aerosol (SOA). The SOA formation potential of individual monoterpenes can vary greatly based on their molecular structure, atmospheric lifetimes, and the volatility of their oxidation products (Atkinson and Arey, 2003; Griffin et al., 1999; Ng et al., 2007a; Zhang et al., 1992). Previous experimental studies of other monoterpenes (such as α-pinene, β-pinene, d-limonene, etc.) have reported SOA yields from ~10% to 50% through OH oxidation and from ~0 to 65% through NO_3 oxidation; among the studied monoterpenes, d-limonene often has the highest reported yields (Mutzel et al., 2016; Griffin et al., 1999; Ng et al., 2007b; Fry et al., 2014). Few studies have been published regarding camphene SOA formation.

Past experimental studies of camphene largely have been focused on gas-phase reactivity with OH, NO_3, and/or O_3 and gas-phase product identification (e.g., Atkinson et al., 1990; Gaona-Colmán et al., 2017; Hakola et al., 1994). Baruah et al. (2018) performed a kinetic and mechanism study of the camphene oxidation initiated by OH radicals using the density functional theory (DFT), in which the rate constant and atmospheric lifetime were reported. It was also suggested that addition at the terminal double bond carbon atom could account for 98.4% of the initial OH-addition. A product study by Gaona-Colmán et al. (2017) showed obvious NO_x dependence in OH + camphene experiments, in which the molar yield of acetone was enhanced by a factor of 3, 33% relative to 10%, in the presence of NO_x (2–2.3ppmv of NO).

Hatfield and Huff-Hartz studied SOA formation from ozonolysis of VOC mixtures, in which the added camphene was considered a non-reactive VOC and assumed to have little to no effect on SOA yields (Hatfield & Hartz, 2011). Mehra et al. (2020) recently published a compositional analysis study of camphene SOA. Although SOA yields were not provided, they demonstrated the potential contribution of highly oxygenated organic molecules (HOMs) and oligomers to camphene SOA formed in an oxidation flow reactor (OFR). Afreh et al. (2020) presented the first mechanistic modeling study of camphene SOA formation. While relatively high SOA yields were reported (with final SOA mass and yields in twice that of α-pinene), no chamber-based SOA data were available for measurement–model comparison at that time.

SOA formation has been shown to be highly dependent on gas-phase NO_x concentrations; and more precisely, the relative ratios of NO:HO_2, hydroperoxyl radicals:RO_2, peroxy radicals (Henze et al., 2008; Ng et al., 2007b; Presto et

al., 2005; Ziemann and Atkinson, 2012; Kroll and Seinfeld, 2008; Song et al., 2005). During chamber experiments, VOCs are subject to oxidation by OH, O_3 and/or NO_3. For some precursors, NO_x levels influence the amount of SOA produced in the initial oxidation steps by controlling the relative proportions of oxidants, the fractional reactivity with

75   those oxidants, and thus the volatility distribution of the products formed (Hurley et al., 2001; Nøjgaard et al., 2006; Kroll and Seinfeld, 2008). For other precursors, NO_x levels influence the amount of SOA produced via fate of RO_2. The reactions between RO_2 and HO_2 form hydroperoxides, which can have sufficiently low volatility to condense into the particle phase. In the presence of NO_x, RO_2 will react with NO, forming organic nitrate and carbonyl compounds that have higher volatilities than the products formed through the HO_2 pathway (Kroll and Seinfeld, 2008; Ziemann

80   and Atkinson, 2012). Previous studies of relatively small compounds (carbon number ≤10), including monoterpenes such as α-pinene, have reported that SOA yields generally increase as initial NO_x decreases, with a proposed mechanism of competitive chemistry between $RO_2 + HO_2$ and $RO_2 + NO$ pathways, of which the latter would form more volatile products (Kroll et al., 2006; Ng et al., 2007; Song et al., 2005). The NO_x dependence of camphene oxidation and SOA formation has been relatively understudied.

85   Here, we present the first systematic study of SOA formation from camphene using laboratory-based chamber experiments and chemically detailed box models. The experiments were conducted at varying NO_x levels and the chamber data were used to provide SOA parameterizations based on the two-product (Odum et al., 1996) and volatility basis set (VBS) modeling approaches (Donahue et al., 2006; Donahue et al., 2009). Two chemically detailed box models, Statewide Air Pollution Research Center (SAPRC) and Generator for Explicit Chemistry and Kinetics of

90   Organics in the Atmosphere (GECKO-A), were used to provide mechanistic insights into the chamber observations and to elucidate the connections between the fate of RO_2 and camphene SOA formation.

2 Methods

2.1 Chamber Facility and Instrumentation

The camphene photooxidation experiments were conducted in the University of California, Riverside (UCR) dual

95   indoor environmental chamber. Chamber characterization and features have been previously described in detail (Carter et al., 2005). Briefly, the UCR environmental chamber consists of two 90 m^3 collapsible Teflon reactors (2mil FEP film) kept at a positive pressure differential (0.015–0.020 in H_2O) to the enclosure where the reactors are located to minimize contamination during experiments. The enclosure is relative humidity controlled (<0.1%), temperature controlled (300 ± 1 K), and continuously flushed with dry purified air (dew point < -40 °C). Prior to and between

100   experiments, reactors were collapsed to a volume < 20 m^3 for cleaning. The cycle of filling-purging the reactors was repeated until particle number concentrations were < 5 cm^{-3} and NO_x mixing ratios were < 1 ppb. The reactors were then flushed with dry purified air and filled up to 90 m^3 overnight. The filling-purging of the reactors is controlled by an "elevator" program in LabView.

NO and NO_2 mixing ratios were monitored by a Thermo Environmental Instruments Model 42C

105   chemiluminescence NO_x analyzer. O_3 mixing ratios were monitored by a Dasibi Environmental Corp. Model 1003-

AH O_3 analyzer. An Agilent 6890 gas chromatograph with flame ionization detector (GC-FID) was used to measure the camphene levels during the experiments.

Multiple instruments were used for particle-phase monitoring. Each reactor was equipped with a scanning mobility particle sizer (SMPS), including a TSI 3081 differential mobility analyzer (DMA), to measure the particle mass concentration. Particle wall loss corrections were performed following the method described in Cocker et al. (2001). Semi-volatile vapor wall losses were assumed to be negligible based on previous measurements made during similar experiments in the UCR CE-CERT chamber of other compounds (such as α-pinene and m-xylene), in which negligible differences were observed between seed and no seed experiments (Clark et al., 2016; L. Li et al., 2015). In addition, stability tests on camphene resulted in negligible vapor wall loss of the parent compound. Particle effective density was directly measured by an Aerosol Particle Mass Analyzer (APM, Kanomax) with a SMPS built in-house (Malloy et al., 2009). Chemical composition of SOA was measured using HR-ToF-AMS (DeCarlo et al., 2006) and analyzed to obtain O:C and H:C ratios by applying the method of Canagaratna et al. (2015). Data processing was performed using the ToF-AMS Analysis Toolkit 1.57 and PIKA 1.16 on Igor Pro 6.36.

2.2 Experimental Conditions

A series of 13 photooxidation experiments of camphene were carried out under varying levels of camphene and NO_x with modeling simulations accordingly (Table 1). Due to the relatively high melting point of camphene (51 °C), camphene (Sigma-Aldrich, purity > 96 %, FG) was injected into a glass manifold (heated to 50 °C by heating tape) using a preheated (~50-55 °C) microliter syringe. As camphene evaporated it was carried to the reactors by dry purified compressed air flowing through a glass manifold at 8 LPM for 15 mins. Injection lines from the glass manifold to the reactors were also heated to reduce losses of camphene. H_2O_2 (Sigma Aldrich, 50 wt.% in H_2O) was injected by adding 200 μl onto glass wool in glass tubing and then placing the tubing in a 56 °C oven with 10 LPM of dry purified compressed air flowing through the tubing for 15 mins and into the reactors. An inert tracer, perfluorohexane (Sigma-Aldrich, 99 %) or perfluorobutane (Sigma-Aldrich, 99 %), was injected to the reactors through the heated glass manifold by a carrier gas of 50 °C pure N_2. NO (Matheson, UHP) at known volume and pressure was transferred and injected through the same glass manifold as the inert tracer. When gaseous injection of camphene, H_2O_2, inert tracer, and NO (when used) was completed, the reactors were internally mixed using built-in blowers to ensure uniform distribution of chemicals, and then irradiated using UV black lights (115w Sylvania 350BL) to start photooxidation. No seed aerosol was used in this study. All experiments were conducted under dry conditions (relative humidity < 0.1 %) at 300 K. The initial conditions of the experiments are summarized in Table 1.

Atmospheric
Chemistry
and Physics
Discussions

Table 1. Summary of initial conditions for chamber experiments and box model simulations.

	Expt.	Initial Conditions for Chamber Experiments and SAPRC Simulations				Initial Conditions for GECKO-A Simulations			
		Camphene (ppb)	Added NO_x (ppb)	*H_2O_2 (ppb)	HC/NO_x (ppb/ppb)	Camphene (ppb)	NO_x (ppb)	H_2O_2 (ppb)	HC/NO_x (ppb/ppb)
without NO_x	WO1	7		854		10		1000	
	WO2	9		1148					
	WO3	28		1212		25		1000	
	WO4	57		1182		50		1000	
	WO5	120		1212		100		1000	
	WO6	223		1576		150		1000	
with NO_x	W1	7	89	854	0.08	10	80	1000	0.13
	W2	25	138	1040	0.18	25	80	1000	0.31
	W3	32	62	1136	0.51				
	W4	43	7	860	5.91	50	80	1000	0.63
	W5	60	94	1227	0.64				
	W6	131	98	1167	1.33	100	80	1000	1.25
	W7	172	60	1121	2.88	150	80	1000	1.88

* H_2O_2 mixing ratio was targeted at 1ppm but corrected base on tracer (perfluorohexane or perfluorobutane) concentration to offset initial reactor volume bias. Corrected H_2O_2 mixing ratios were used in SAPRC modeling.

2.3 Model Configurations and Conditions

140   The chamber experiments were modeled using two different box models, SAPRC and GECKO-A. The SAPRC model was chosen because it has been designed to evaluate gas-phase chemistry in the UCR chamber. The GECKO-A model was chosen because of the ability to predict both gas and particle phase composition, and the prior work of Afreh et al. (2020), in which GECKO-A was used to study SOA formation from camphene.

2.3.1 SAPRC

145   A gas-phase oxidation mechanism was derived using the SAPRC mechanism generation system (MechGen) with modified initial rate constants (camphene with OH, NO_3 and O_3) based on published literature data (Atkinson et al., 1990). MechGen, described elsewhere (Carter, 2021; Carter, 2020b; Jiang et al., 2020), is capable of generating fully explicit mechanisms for the atmospheric reactions of many types of organic compounds and the intermediate radicals they form. MechGen uses experimentally derived rate constants and branching ratios if data are available and

150   otherwise uses estimated rate constants and branching ratios based on group additivity and other estimation methods. This system was used to derive reactions of explicit and lumped organic compounds and products in the development of the SAPRC-18 mechanism (Carter, 2020a) and a detailed SAPRC furans mechanism (Jiang et al., 2020).

The MechGen-derived camphene mechanism was implemented into the SAPRC box model to simulate chamber experiments under the same chemical conditions as the chamber experiments, where the initial hydrocarbon concentrations and NO_x levels were as defined in Table 1. The SAPRC box model system has been used for chemical

155   mechanism development, evaluation, and box modeling applications since the mid-1970s (Carter, 1990, 1994, 2000,

2010a, 2010b, 2020a). The initial conditions and relevant chemical parameters for environmental chamber experiments are required inputs; simulations can be performed using multiple versions of the SAPRC gas-phase chemical mechanism. In this work, the recently published version, SAPRC-18 (Carter, 2020a), was selected as the

160   base mechanism because it represents the current state of the science and includes the most up-to-date model species and explicit representation of RO_2 chemistry.

2.3.2 GECKO-A

GECKO-A is a nearly explicit mechanism generator and SOA box model. GECKO-A relies on experimental data and structure-activity relationships (SARs) to generate detailed oxidation reaction schemes for organic compounds. The

165   generated reaction schemes are applied in the SOA box model to simulate SOA formation based on the absorptive gas/particle partitioning model of Pankow (1994), where thermodynamic equilibrium between the gas and an ideal particle phase is assumed. Detailed descriptions of GECKO-A, including mechanism generation and SOA formation, are provided by Aumont et al. (2005) and Camredon et al. (2007). GECKO-A has been used to predict SOA in a number of studies (e.g., Aumont et al., 2012; Lannuque et al., 2018; McVay et al., 2016), including camphene (Afreh

170   et al., 2020). Details of the camphene mechanism and SOA box modeling were described in Afreh et al. (2020). Briefly, the camphene mechanism includes 1.3×10^6 reactions and 1.8×10^5 oxidation products; vapor pressures of products were calculated based on the Nannoolal method (Nannoolal et al., 2008).

In this work, the initial conditions for the GECKO-A simulations were chosen to best represent idealized chamber conditions; that is, initial camphene and NO_x mixing ratios were fixed based on target values for the chamber

175   experiments and not modified to reflect actual values used. GECKO-A simulations were performed under two NO_x conditions, with 80 ppb of NO_x and without NO_x (Table 1). For both NO_x conditions, the initial hydrocarbon mixing ratios were set at 10, 25, 50, 100, and 150 ppb. All simulations were run under the following initial conditions: 1000 ppb of H_2O_2, 1 µg m^{-3} of organic seed with molecular weight of 250 g mol^{-1}, 298 K temperature, 1% relative humidity, and 50° solar zenith angle (required to compute the photolysis frequencies). Simulation results for camphene were

180   compared with chamber data including SOA yield, precursor decay rates, and oxidant levels.

3. Experimental and Modeling Results

Table 2 summarizes the measured initial NO/NO_2 mixing ratios, initial camphene concentration ($[HC]_0$), reacted camphene concentration ($\Delta[HC]$), SOA mass (M_o) formed, particle density, final peak particle diameter (d_p), photochemical aging time, irradiation time, and SOA yield for all 13 experiments. Measured and predicted gas-phase

185   species are presented in Sect. 3.1; SOA mass and yields are presented in Sect. 3.2. The predicted fate of RO_2 in the context of initial HC to initial NO_x mixing ratio ($[HC]_0/[NO_x]_0$) is presented in Sect. 3.3.

**Table 2.** Chamber SOA data, WO indicates experiments without added NO_x and W with added NO_x.

Expt.	Initial NO/NO$_2$	[HC]$_0$	Δ[HC]	M_o	PM den.	Peak d_p	Irradiation time	Photochemical aging time	Yield
	ppb	µg m^{-3}	µg m^{-3}	µg m^{-3}	g cm^{-3}	nm	hour	hour	
WO1	0/0	41	41	6.1	1.42	126	4.9	16.1	0.15
WO2	0/0	49	49	3.7	1.42	125	5.0	16.7	0.08
WO3	0/0	155	153	42.0	*1.36	214	6.1	17.7	0.27
WO4	0/0	313	305	84.4	*1.34	270	6.7	15.8	0.28
WO5	0/0	663	597	158.6	1.30	286	6.7	9.5	0.27
WO6	0/0	1230	844	162.4	*1.31	492	6.1	5.0	0.19
W1	86/2	40	40	14.6	1.46	120	5.1	50.6	0.36
W2	114/24	140	140	46.1	1.47	188	5.2	40.6	0.33
W3	51/11	177	177	112.3	*1.44	185	6.0	42.0	0.64
W4	5/2	238	237	96.0	1.35	290	5.9	16.1	0.41
W5	45/49	334	334	199.5	*1.44	430	5.8	33.6	0.60
W6	42/56	724	724	428.8	*1.42	665	5.8	12.7	0.59
W7	45/15	956	950	494.3	*1.39	800	6.4	8.75	0.52

* Estimated using best fit line shown in Fig. S6.

3.1 Gas-Phase Reactivity

Figure 1 shows measured and predicted camphene consumption for the 13 photooxidation experiments, and the calculated time-dependent β values (ratio of $RO_2 + NO$ to the sum of $RO_2 + NO$ and $RO_2 + HO_2$)(Henze et al., 2008; Pye et al., 2010) based on SAPRC predictions for each experimental condition. Additional comparisons of measured and predicted gas-phase species are shown in Fig. S1 and Fig. S2. Higher camphene decay rates and higher OH levels (0.15–0.88 ppt with added NO_x; 0.05–0.29 ppt without added NO_x) were observed and predicted for experiments with added NO_x than without; likely due to the fast recycling of OH when NO_x was present (Fig. 1). For all experiments, the β values changed as a function of time due to changing chemical conditions. Note that due to off-gassing of NO_x from the Teflon reactor (Carter et al., 2005), β values simulated here were larger than 0 even for experiments without added NO_x. Experiments with added NO_x have β values from 0.12–1, while experiments without added NO_x have values < 0.12. For all parameters (camphene consumption, NO_x decay, O_3 formation, and OH levels), the SAPRC simulation results were generally in good agreement with the experimental data. This consistency between experimental data and SAPRC simulations supports the use of the MechGen generated gas-phase camphene mechanisms and SAPRC box model results to interpret chamber observations.
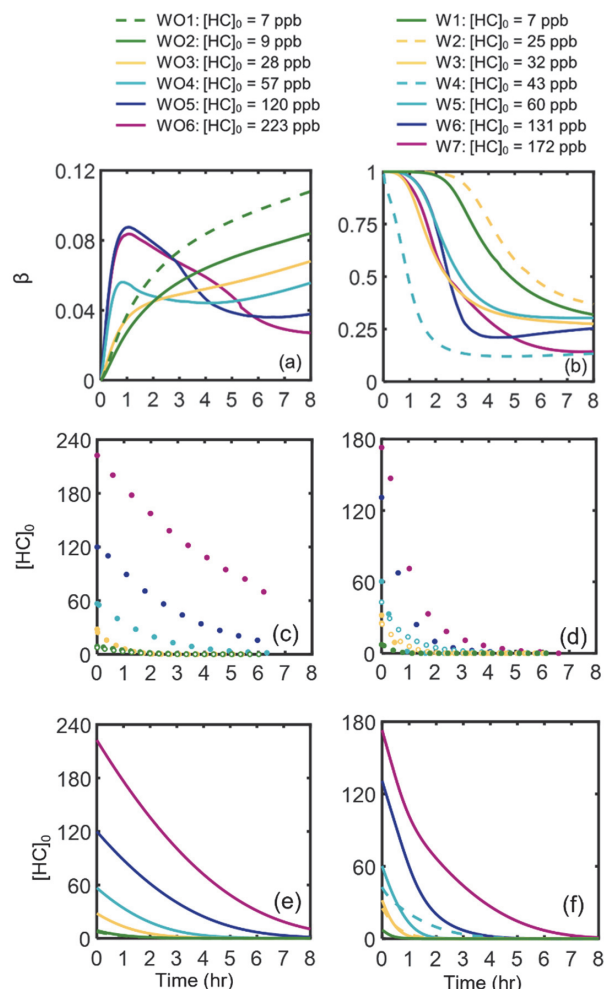
Figure 1. SAPRC predicted β values: (a) without added NO_x, and (b) with added NO_x. Measured camphene consumption as a function of irradiation time: (c) without added NO_x, and (d) with added NO_x. SAPRC predicted camphene consumption: (e) without added NO_x, and (f) with added NO_x. The hollow makers used in (c) and (d) are equivalent to dashed lines defined in the legends.

3.2 SOA Mass and Yield

Measured SOA yields (SOA mass formed, M_o/hydrocarbon reacted, ΔHC) are shown in Fig. 2 as a function of SOA mass (M_o) for experiments with (solid circles) and without (solid squares) added NO_x. The SOA yields were much higher in experiments with added NO_x (0.33–0.64) than experiments without added NO_x (0.08–0.28). The observed trends in SOA yields were unexpected based on prior chamber studies of SOA formation from monoterpenes, such as OH oxidation studies of α- and β-pinene, in which SOA yields were reported to be suppressed under high-NO_x conditions (Eddingsaas et al., 2012; Pullinen et al., 2020; Sarrafzadeh et al., 2016).
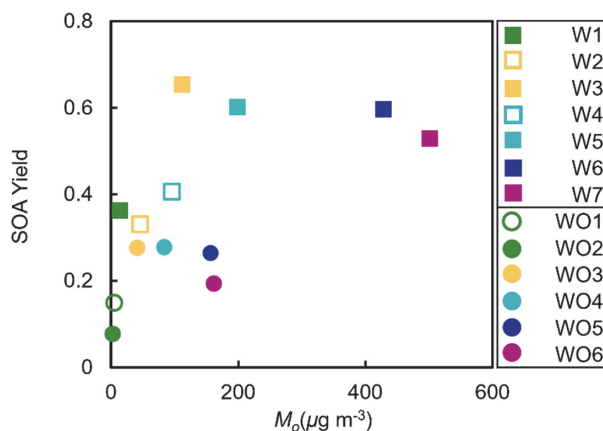
Figure 2. Measured camphene SOA yields as a function of SOA mass (M_o). Squares indicate experiments with (W) and circles without (WO) added NO_x. Initial HC mixing ratios are differentiated by color; open symbols are used to indicate
220 **replicate initial HC mixing ratios.**

Figure 2 shows another unexpected observation: the SOA yields decreased at high SOA mass under both NO_x conditions, which was captured in the measurements and also in the GECKO-A model simulations (see Sect. 5). In the presence of NO_x, the observed SOA yields increased with M_o for $M_o \leq 112$ µg m^{-3}, plateaued between 112 µg m^{-3} $< M_o \leq 429$ µg m^{-3}, and then decreased for $M_o > 429$ µg m^{-3}. Without NO_x, the observed SOA yields increased for M_o
225 ≤ 42 µg m^{-3}, plateaued between 42 µg m^{-3} $< M_o \leq 159$ µg m^{-3}, and then decreased for $M_o > 159$ µg m^{-3}. These unexpected trends in SOA yields were further investigated using the SAPRC and GECKO-A box models (Sect. 4 & 5).

The varying [OH] levels in the chamber experiments led to a wide range of photochemical aging times, from hours to days. The irradiation time was converted to equivalent photochemical aging time in the ambient atmosphere using
230 equation (1) (Aumont et al., 2012):

$$\tau = \frac{1}{[OH]_{atm}} \int_0^t [OH]_{sim} dt \qquad (1)$$

where $[OH]_{atm}$ was assumed to be 2×10^6 molecule cm^{-3}. Figure 3 shows the measured SOA yields as a function of photochemical aging time calculated using OH values predicted by SAPRC ($[OH]_{sim}$). The SOA yields in experiments with and without added NO_x are dependent on OH levels and thus photochemical aging time. Higher $[HC]_0$ generally
235 led to steeper increases in SOA yield as a function of aging time. Experiments with added NO_x generally had longer photochemical aging times than experiments without added NO_x. In addition, in experiments with added NO_x, the yield curves mostly plateaued by the end of the experiment; however, in most of the experiments without added NO_x, the yield curves were still increasing at the end of the experiments. The higher SOA yields in experiments with added NO_x may partially be attributed to the difference in [OH] levels and extents of aging. Similar NO_x effects have been
240 reported in many previous studies (e.g., Ng et al., 2007a; Sarrafzadeh et al., 2016). Sarrafzadeh et al. (2016) proposed that in a study of β-pinene the OH level was the main factor that accounted for differences in SOA yields under varying

$[NO_x]_0$. In the camphene experiments presented herein, except for some of the experiments without added NO_x, the aging effects were determined to be less important than RO_2 chemistry, since the SOA yield curves as a function of photochemical aging already plateau or nearly plateau by the end of experiments (Fig. 3).
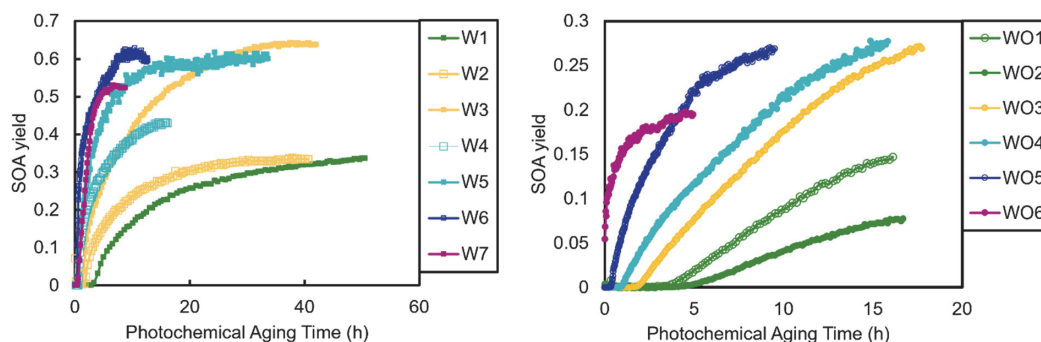

245

Figure 3. Measured SOA yields as a function of photochemical aging time in experiments with added NO_x (a); and experiments without added NO_x (b).

SOA yields were shown as a function of $\Delta[HC]$, $[HC]_0/[NO_x]_0$, and photochemical aging time in Fig. 4. For the experiments without added NO_x, a constant value of 1 ppb was used in the calculations of $[HC]_0/[NO_x]_0$ to account

250 for NO_x off-gassing from the Teflon reactors. Based on recent characterization experiments, the UCR chamber has a NO_x off-gassing rate of 2.8 ppt/min in the form of HONO; the camphene experiments lasted for ~300 to 360 mins. Over low $\Delta[HC]$ range, when $\Delta[HC]$ increases, SOA yield increases as well. When $\Delta[HC]$ is larger than approximately 200 ug m^{-3}, this correlation becomes less apparent, due to the high sensitivity of SOA formation on $[HC]_0/[NO_x]_0$ over the range of $\Delta[HC]$ sampled. At a given $\Delta[HC]$ level, a relatively smaller $[HC]_0/[NO_x]_0$ (when it was within 0.5–200)

255 would lead to a higher SOA yield (decreasing $[HC]_0/[NO_x]_0$ by approximately 100 times may double the SOA yield). The chamber data presented here exhibit a general trend that, under the regular regime (distinguished from the extreme $[NO_x]$ regime), higher SOA yields are observed from camphene oxidation at higher $\Delta[HC]$ and smaller $[HC]_0/[NO_x]_0$. This is different from studies of α-pinene, in which smaller $[HC]_0/[NO_x]_0$ generally led to smaller SOA yield (Eddingsaas et al., 2012).
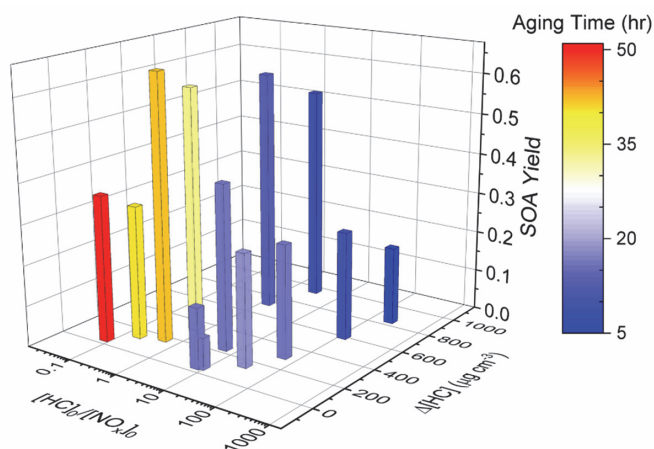
260

Figure 4. SOA yield dependence on $[HC]_0/[NO_x]_0$, $\Delta[HC]$, and photochemical aging time.

3.3 $[HC]_0/[NO_x]_0$ and the Fate of Peroxy Radicals

Table S1 shows the experimental $[HC]_0/[NO_x]_0$ and the SAPRC predicted fate of total RO_2 (the summation of all the RO_2 radicals formed from camphene and camphene products) for all the chamber runs. In Fig. 5, the fate of total RO_2

265 is shown as a function of $[HC]_0/[NO_x]_0$. The majority of RO_2 was predicted to undergo bimolecular reactions with HO_2 or NO across the range of $[HC]_0/[NO_x]_0$ values sampled. At $[HC]_0/[NO_x]_0 < 6$, $> 50\%$ of the RO_2 was predicted to react with NO; and at $[HC]_0/[NO_x]_0 > 10$, $> 50\%$ of the RO_2 was predicted to react with HO_2. A roughly 50:50 branching of RO_2 between NO and HO_2 was reached when $[HC]_0/[NO_x]_0$ was 6:1, which is close to the ratio that was suggested in Presto et al. (2005). When $[HC]_0/[NO_x]_0$ increased over 50, the total fraction of bimolecular $RO_2 + RO_2$

270 and unimolecular RO_2 reactions increased from 0 to 40%. In addition, the normalized total RO_2 concentration (accumulated total $[RO_2]/[HC]_0$, ppbv/ppbv) increased as $[HC]_0/[NO_x]_0$ decreased (Fig. 4 and Fig. 6). There is a general trend of increasing SOA yield with decreasing $[HC]_0/[NO_x]_0$ (Fig. 4 and Fig. 6), with the exception of four outliers (W1, W2, WO1, and WO2) that have relatively low SOA yields. Experiments WO1, WO2, W1 had the lowest $\Delta[HC]$ (49, 41, and 40 $\mu g/m^3$, respectively, Table 2), indicating the SOA yields were influenced by $\Delta[HC]$ as well as

275 RO_2 chemistry. The connections between the fate of RO_2 and observed SOA yields are further discussed in Sect. 4.
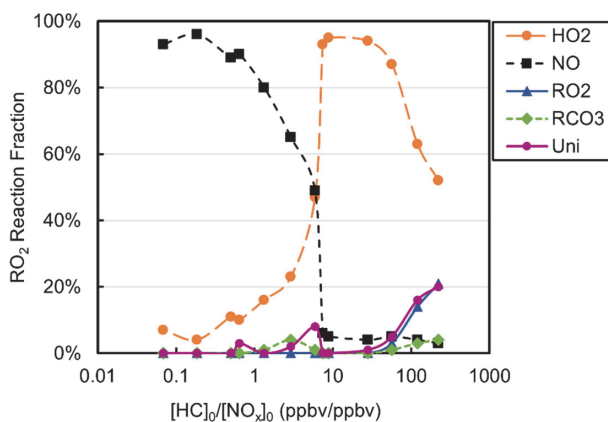
Atmospheric
Chemistry
and Physics
Discussions

Figure 5. Fractions of total RO_2 reactions of each type as a function of $[HC]_0/[NO_x]_0$ based on Table S1.
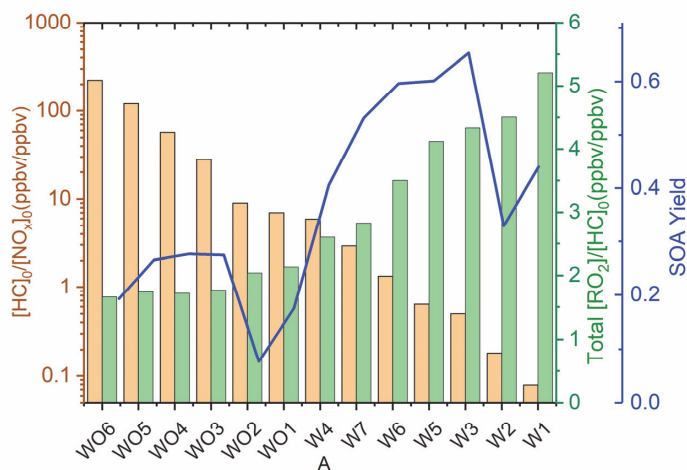

Figure 6. Relationship between accumulated total $[RO_2]/[HC]_0$, $[HC]_0/[NO_x]_0$, and SOA yields.

280   By assuming the gas-phase chemistry and product distribution were similar when $RO_2 + NO$ accounted for more than 80% of the total RO_2 consumption and when $RO_2 + HO_2$ accounted for more than 80% of the total RO_2 consumption, experiments with (W1–3, 5–6) and without (WO1–4) added NO_x were grouped and used to derive SOA parameters using the two-product (Odum et al., 1996) and VBS approaches (Donahue et al., 2006; Donahue et al., 2009). The resultant parameters are shown in Table 3 and Table 4.

285   **Table 3.** Two-Product Model SOA parameters.

	α_1	$\log_{10} C^*_1$	α_2	$\log_{10} C^*_2$
Without NO_x	0.0017	1.08	0.3139	0.92
With NO_x	0.4484	1.77	0.2398	-2.94

Table 4. VBS Model SOA parameters.

$\log_{10} C^*$	$^\dagger \alpha_{wo}$	$^\dagger \alpha_w$
0.1	0.0001	0.2657
0	0.0152	0.0008
10	0.3069	0.0357
100	0.0001	0.4222
1000	0.0003	0.0000

† wo refers to without added NO_x; w refers to with added NO_x.

4 Discussion

The reaction rate constant of camphene with O_3 is relatively low compared to OH, and thus it is expected that OH is
the dominant oxidant in the photooxidation of camphene under chamber conditions; especially with the high initial
H_2O_2 (~1 ppm) concentrations. This is supported by SAPRC simulation results (see Fig. S3 in SI), in which SAPRC
predicted that O_3 accounts for 0–3% and NO_3 for 0–16% of camphene oxidation, demonstrating the important role of
OH oxidation in these studies.

4.1 Camphene + OH Gas-phase Mechanism

Figure 7 shows the MechGen predicted reactions and products of OH-initiated oxidation of camphene in the presence
of NO_x through one major pathway, which had a yield of 0.83 (a more detailed reaction mechanism schematic is
presented in Fig. S4). The reaction starts with OH addition to the $CH_2=(C)$ position to form a ring-retaining alkyl
radical, which further reacts with O_2 to form the camphene peroxy radical, RO_2-a. RO_2-a can react with oxidants (NO,
NO_3, HO_2, and/or other RO_2) to create an alkoxy radical, RO-a, with NO to NO_2 conversion; or form stable products
such as organic nitrate (NO3CAMP1), hydroperoxide (HO2CAMP1), and phenolic (RO2CAMP1) compounds. The
cyclic alkoxy radical RO-a can undergo prompt beta (β)-scission ring-opening reaction, and then O_2 addition to form
another peroxy radical, RO_2-b. In the presence of NO_x, rapid β-scission decomposition, or ring-opening reactions of
the camphene alkoxy radicals (RO-b and RO-c) occur through the RO_2 + NO pathway, leading to the generation of
the proxy radical RO_2-d with lower carbon number and higher O:C ratio (increases from 0.30 for RO_2-a to 0.71 for
RO_2-d).

Figure 7. Schematic of the OH-initiated oxidation of camphene mechanism in SAPRC at 298 K and atmospheric pressure in the presence of NO_x. Check Fig. S4 for more details.

MechGen predicted that RO_2-d could undergo 1,5 H-shift isomerization nearly instantaneously, even in the presence of ~ 100 ppb NO_x. Subsequent rapid addition of O_2 can form a new peroxy radical RO_2-d* which could undergo 1,7 H-shift isomerization and form the peroxy radical RO_2-d**. RO_2-d** can participate in termination reactions with NO and HO_2 to form organic nitrate (NO3CAMP4) and hydroperoxide (HO2CAMP4) products, which are known as highly oxygenated organic molecules (HOMs). In the presence of NO_x, RO_2-d** can also react with NO to form the alkoxy radical RO-d that can undergo 1,4 H-shift isomerization and then O_2 addition to form the new peroxy radical RO_2-e which will also lead to the formation of HOMs such as NO3CAMP5, HO2CAMP5, and UNICAMP. A recent SOA study by Mehra et al. (2020) demonstrated the formation of HOMs in camphene chamber experiments under both low NO_x (30 ppb camphene, ~ 0 ppb NO_x) and medium NO_x (30 ppb camphene, 2.2 ppb NO, 58.4 ppb NO_2) conditions. Based on their observations and analysis, the average molecular formula of the camphene SOA was $C_{7.26}H_{9.85}O_{4.03}$ for low NO_x and $C_{6.63}H_{9.7}N_{0.12}O_{4.21}$ for the medium NO_x conditions, which also suggested the occurrence of ring-opening and decomposition reactions during camphene photooxidation, as predicted by MechGen.

4.2 The Formation of HOMs and Influence on SOA Yields

Table 5. Log_{10} $C*$ value for selected 1st generation products.

Species	Atom				O:C	$\log_{10} C*$	Species	Atom				O:C	$\log_{10} C*$
	C	H	O	N				C	H	O	N		
HO2CAMP1	10	18	3	0	0.30	2.5	NO3CAMP1	10	17	4	1	0.40	3.5
HO2CAMP2	10	18	4	0	0.40	1.7	NO3CAMP2	10	17	5	1	0.50	2.6
HO2CAMP3	7	12	4	0	0.57	2.5	NO3CAMP3	7	11	5	1	0.71	3.5
HO2CAMP4	7	12	7	0	1.00	-1.3	NO3CAMP4	7	11	8	1	1.14	-0.1
HO2CAMP5	7	12	8	0	1.14	-4.3	NO3CAMP5	7	11	9	1	1.29	-2.8
RO2CAMP1	10	18	2	0	0.20	3.8	NOCAMP1	6	10	4	0	0.67	2.6
UNICAMP	7	10	7	0	1.00	-3.9	NOCAMP2	7	10	7	0	1.00	-1.1

Table 6. Fractions of peroxy radical RO_2-a reactions of each type, calculated based on SAPRC simulations.

Expt.	$[HC]_0$	$*[HC]_0/[NO_x]_0$	SOA Yield	Fraction of RO_2-a Reaction				
	(ppb)	(ppbv/ppbv)		NO	HO_2	RCO_3	RO_2	NO_3
WO1	7	7	0.15	0.03	0.97	0	0	0
WO2	9	9	0.08	0.02	0.98	0	0	0
WO3	28	28	0.27	0.02	0.97	0	0	0
WO4	57	57	0.28	0.03	0.89	0	0.08	0
WO5	120	120	0.27	0.03	0.64	0.02	0.30	0
WO6	223	223	0.19	0.03	0.54	0.02	0.41	0
W1	7	0.08	0.36	1.00	0	0	0	0
W2	25	0.18	0.33	1.00	0	0	0	0
W3	32	0.51	0.64	0.97	0.03	0	0	0
W4	43	5.91	0.41	0.46	0.53	0.01	0	0
W5	60	0.64	0.60	0.97	0.03	0	0	0
W6	131	1.33	0.59	0.88	0.12	0.01	0.01	0
W7	172	2.88	0.52	0.65	0.30	0.03	0.01	0

*The $[HC]_0/[NO_x]_0$ for WO1–6 experiments were estimated assuming 1 ppb of NO_x.

325   Table 5 lists the log $C*$ values and O:C ratios for the major camphene products predicted; vapor pressures of products were calculated based on the Nannoolal method (Nannoolal et al., 2008). HOMs have much lower volatilities than the earlier terminal products such as NO3CAMP1, HO2CAMP1, and RO2CAMP1. HOMs formed by autoxidation steps in camphene radical chain reactions are mediated by the H-shift isomerization of RO_2-d and RO-d. Table 6 shows the SAPRC predicted fate of RO_2-a for all chamber runs; the fate of summed RO_2 is shown in Table

330   S1, which includes RO_2-a~d and all the RO_2 radicals formed from other minor pathways. For the experiments without added NO_x (WO1–6), once the initial peroxy radical RO_2-a was formed, a large fraction of RO_2-a (0.54-0.98) quickly reacted with HO_2 to form the terminal product HO2CAMP1, while only 2–3% of RO_2-a reacted through the NO pathway and led to the generation of HOMs. For the experiments with added NO_x (W1–7), much higher RO_2-a + NO fractions (0.65–1.00) were predicted by SAPRC. The fates of summed RO_2 also suggested that not only RO_2-a, but

335   also the other RO_2 radical intermediates would tend to favor further reactions through the NO reaction chain to form lower volatility products.

Based on the predicted fate of RO_2 in SAPRC simulations, the higher SOA yields in experiments with NO_x were due to the formation of HOMs through autoxidation in the presence of NO_x. In general, faster RO_2 reaction with NO, HO_2 or other RO_2 limits HOM formation by autoxidation (Bianchi et al., 2019). In previous monoterpene SOA studies,

340   HOM formation was often observed when NO_x was absent or under lower NO_x conditions (Pye et al., 2019; Schervish and Donahue, 2020; Zhao et al., 2018). For example, Zhao et al. (2018) demonstrated that autoxidation for some RO_2 is competitive with RO_2 + NO at ppb levels of NO for O_3-initiated α-pinene oxidation. They also reported that HOM formation decreased as the initial NO concentration increased from 0 ppb to 30 ppb. In the camphene experiments presented herein, the reverse trend was observed (see experiments WO4, W4 and W5 conducted with ~50 ppb

camphene at different NO_x levels). This was due to the key RO_2 species, RO_2-d, which was predicted to form only in the presence of NO_x and had a fast enough autoxidation rate constant to effectively compete with bimolecular reactions.

The decreasing SOA yields at high $[HC]_0$ and M_o in all experiments (shown in Fig. 2) can also be explained by RO_2 chemistry. For experiments with added NO_x, the decreasing SOA yield trend was most likely due to the shift of RO_2 reaction pathways from NO to HO_2. The fraction of RO_2-a + NO decreased from 0.97 (W5) to 0.65 (W7) while the fraction of RO_2-a + HO_2 increased from 0.03 (W5) to 0.23 (W7). For the experiments without NO_x, the shift from RO_2 + HO_2 to self- and cross-reactions of RO_2 at high $[HC]_0$ and M_o led to decreasing SOA yields. When $[HC]_0$ increased from 57 ppb to 223 ppb, the fractions of RO_2-a + HO_2 decreased from 0.89 (WO4) to 0.54 (WO6) and the fraction of RO_2-a + RO_2 increased by a factor of five, from 0.08 to 0.41. Moreover, this shift from bimolecular reactions with HO_2 to RO_2 as $[HC]_0$ increased also occurred in the context of the total RO_2 (Table S1). Generally, products that were predicted to form from one RO_2 reacting with another RO_2 in the absence of NO_x, had relatively higher volatility than those formed from that RO_2 reacting with HO_2; for example, RO2CAMP1 formed from RO_2-a + RO_2 was more volatile than HO2CAMP1 formed from RO_2-a + HO_2 (Table 5). The increasing fraction of self- and cross-reactions of RO_2 therefore is one likely explanation for the decreasing SOA yields at high ΔHC and M_o in the experiments without NO_x.

In experiments W1 and W2, the relatively low SOA yields (0.36 and 0.33) can be partially attributed to differences in product distribution. A comparison of the product distributions between W1, W2, W3 and W5 suggested similar yields of NO3CAMP1–5 and NOCAMP1–2, but major differences in yields of UNICAMP and HO2CAMP1–5 (Fig. S5). Experiments W3 and W5 were selected for comparison because of their closest total RO_2 fractional reaction distribution (approximately 90% RO_2 + NO and 10% RO_2 + HO_2) to W2 (96% RO_2 + NO and 4% RO_2 + HO_2) and W1 (93% RO_2 + NO and 7% RO_2 + HO_2) but higher SOA yield (0.64 and 0.6). W1 and W2 were predicted to have much smaller SOA yield than W3 and W5 in the low volatility products HO2CAMP1-5 (especially product HO2CAMP5, the lowest volatility among all listed products in Table 5, $\log_{10}C^* = -4.3$) and UNICAMP (the second lowest volatility shown in Table 5, $\log_{10}C^* = -3.9$), which can contribute to the lower SOA yield. Further analysis of W1 and W2 revealed a likely cause for the different yields of HO2CAMP1–5 and UNICAMP. W1 and W2 were predicted to have delayed peaks of [OH] (after 3–4 hours of irradiation) which likely was due to the high NO_x concentrations (Fig. S2). Correspondingly, the $[HO_2]$ was highly suppressed during the first 2 hours of irradiation. Under high $[NO_x]$, the RO_2-e + HO_2 pathway shown in Fig. 7 therefore could be suppressed, resulting in a lower yield of HO2CAMP5. This indicates a second regime may exist at high $[NO_x]$ and significantly lower $[HC]_0/[NO_x]_0$.
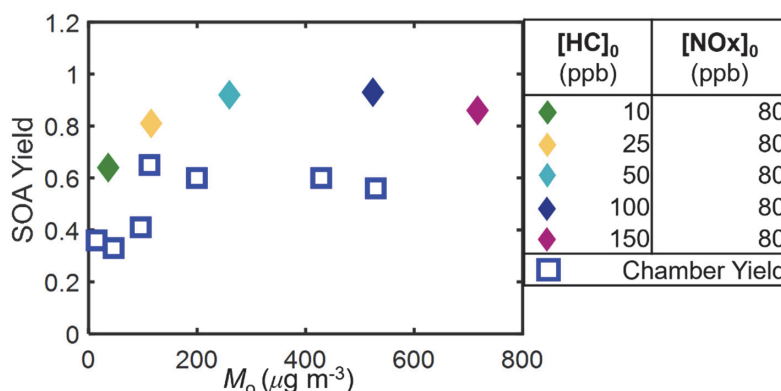
5 GECKO-A simulations

5.1 SOA Mass and Yield

The comparison of gas- and particle-phase species between chamber experiments and GECKO-A model simulations are shown in Fig. S1 and Fig. S2. Without added NO_x, GECKO-A predicts much smaller camphene consumption rates and no formation of O_3, while both the chamber data and SAPRC simulations suggest a final O_3 mixing ratio of ~10 ppb (Fig. S1). This may be due to an underrepresentation of data and relevant pathways for low to no NO_x conditions

Atmospheric
Chemistry
and Physics
Discussions
Open Access

EGU

380   in the GECKO-A mechanism generation system, and the incomplete treatment of wall effects in the application of the
GECKO-A box model. The without added NO_x simulations are not further discussed. With added NO_x, GECKO-A
shows good agreement with the experimental data and SAPRC simulations in the context of camphene consumption,
O_3, and OH levels.

385   **Figure 8. Predicted SOA yields based on GECKO-A model simulations.**

Figure 8 shows the predicted SOA yields based on GECKO-A. For simulations with added NO_x, while the model
predicted higher SOA yields (0.64–0.93) than were observed (0.33–0.64), the trends in the SOA yields were similar
between chamber observation and simulations. The simulated SOA yield increased with SOA mass for SOA mass <
$260 \mu g \ m^{-3}$, plateaued for SOA mass between 260 and 524 $\mu g \ m^{-3}$, and then decreased for SOA mass > 524 $\mu g \ m^{-3}$.

390   The decreasing trend in SOA yields is represented in the predicted and measured O:C ratio (Fig. 9). The average
carbon number used in this study was defined as the mole-weighted averaged carbon number for the main products
(~95% by mass). The calculation was based on equation (2), where nC_i, $M_{o,i}$, and MW_i are the carbon number, mass,
and molecular weight of species i, respectively.

$$\text{Average carbon number} = \frac{\sum_i \frac{nC_i \times M_{o,i}}{MW_i}}{\sum_i \frac{M_{o,i}}{MW_i}} \tag{2}$$

395   With added NO_x, the average carbon number of both the particle and gas phase increases as $[HC]_0$ increases (Fig. 9).
Higher average product carbon numbers suggest that less oxygenated products with smaller O:C (higher volatility)
were formed. The average vapor pressure of products may then increase as $[HC]_0$ increases, reducing the SOA yield.
This is consistent with the chamber results and could contribute to the decreasing SOA yield at higher mass loadings
(M_o > 524 $\mu g \ m^{-3}$) in Fig. 8. In addition, the GECKO-A simulation of 150 ppb HC with NO_x predicts the highest

400   fraction of precursor reacted by O_3 and NO_3 among all 5 runs, suggesting a large fraction of nitrogen-containing
products (Fig. S7). Available AMS data suggest a clear difference in the abundance of nitrogen-containing species
between the experiments with and without added NO_x. NO_3 was predicted to account for an average ~14% of total
SOA mass in simulations with NO_x, and only 1% of total SOA without NO_x.
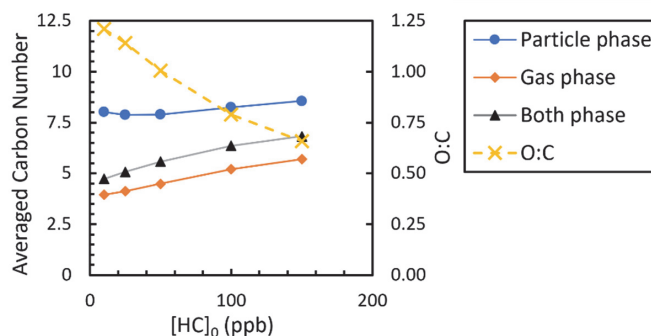
Figure 9. Predicted particle O:C and mole-weighted averaged carbon number of products with added NO_x by GECKO-A.

5.2 Particle Density and O:C

Figure 10a shows the GECKO-A predicted O:C ratio and measured O:C ratio as a function of $[HC]_0/[NO_x]_0$ for all experiments. A good agreement in O:C ratios was observed between the model predictions and chamber data. The O:C ratio decreased from 1.21 to 0.39 as $[HC]_0/[NO_x]_0$ increased from 0.13 to 223, supporting that more highly oxygenated products were formed at lower $[HC]_0/[NO_x]_0$.
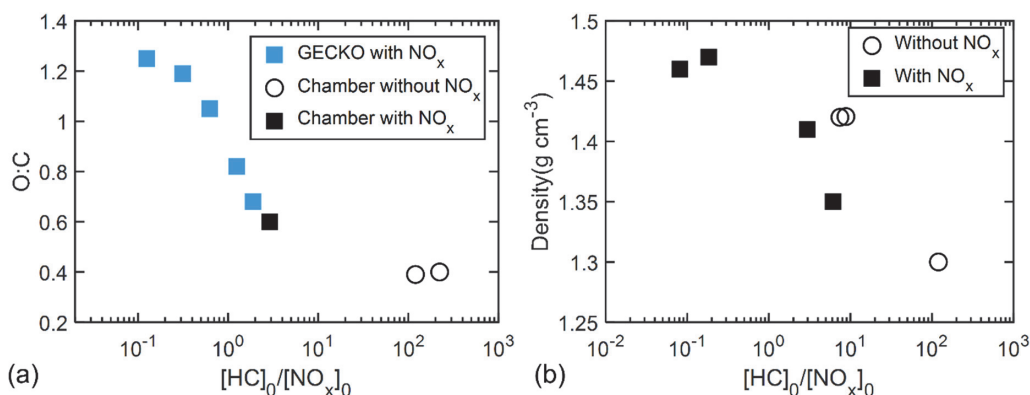
Figure 10. (a), O:C ratio as a function of $[HC]_0/[NO_x]_0$ with AMS data and prediction by GECKO-A simulation. (b), Particle density (directly measured by APM–SMPS) shown as a function of $[HC]_0/[NO_x]_0$.

A negative correlation was also observed between measured particle density and $[HC]_0/[NO_x]_0$. The final density of particles decreased from 1.47 g cm^{-3} to 1.30g cm^{-3} as $[HC]_0/[NO_x]_0$ increased from 0.08 to 120 (Fig.10b). The change in O:C ratio could account for the change in density. O:C and H:C have been used in SOA density prediction by semi-empirical equation (Nakao et al., 2013; Kuwata et al., 2012), in which O:C plays a dominant role in determining organic particle density compared to H:C. Consistent with the semi-empirical formulations, the density of particles formed from oxidation of camphene increased as O:C (ranged from 0.39 to 1.21) increased, while H:C varies over a small range (from 1.42 to 1.79). The change in density supports the proposed explanation that more oxygenated products were formed under lower $[HC]_0/[NO_x]_0$. The wide range in final density and the correlation with

[HC]$_0$/[NO$_x$]$_0$ shown here is reported for the first time. The SOA mass of each experiment in this study was calculated with its own density of SOA, instead of applying an averaged density. A list of particle densities used in this study can be found in Table 2.

6 Conclusions

Here we present for the first time SOA yields from oxidation of camphene based on experiments performed in UCR environmental chamber with varying [NO$_x$]$_0$. Higher SOA yields were measured with added NO$_x$ (0.33–0.64) than without added NO$_x$ (0.08–0.26) generally at atmospherically relevant OH concentration. SOA formation from oxidation of camphene showed different NO$_x$ dependence from other known monoterpenes (e.g., α-pinene, d-limonene) and other n-alkanes (carbon≤ 10), in studies of which higher SOA yields were measured when [NO$_x$] was low. Here, higher Δ[HC] and lower [HC]$_0$/[NO$_x$]$_0$ (within 0.5–200) generally led to higher SOA yields. Similar NO$_x$ dependence of camphene oxidation has been found with two sesquiterpenes (longifolene and aromadendrene) but was attributed to the production of nonvolatile organic nitrates with no detailed mechanistic analysis provided at that time (Ng et al., 2007b).

Although [HC]$_0$/[NO$_x$]$_0$ shows clear correlation with SOA yield but cannot represent the RO$_2$ chemistry completely. The dependence of SOA yields on HC and NO$_x$ can be explained by RO$_2$ chemistry and the competition between varying bimolecular RO$_2$ and unimolecular RO$_2$ reaction pathways generated using SAPRC MechGen. The RO$_2$ + NO pathway favored in experiment with added NO$_x$ led to the highest production of RO$_2$ and formed HOMs products with much lower volatilities than products from other pathways. In addition to the regular regime introduced above, our study suggested an extreme regime where significantly high [NO$_x$] may suppress the SOA yield. High NO$_x$ concentration may suppress the HO$_2$ concentration at the beginning of the reactions, causing the reduction in yield of low volatility products such as UNICAMP and HO2CAMP5. This indicates that if the reactions happened under NO$_x$-rich environment with extremely high ratio of NO to HO$_2$ (HO$_2$/NO), the SOA yield from oxidation of camphene could possibly be significantly suppressed. Simulations with chemically detailed box models such as SAPRC are recommended in identifying SOA formation regimes. Constant β values controls are preferred to be applied in future SOA formation study of monoterpenes to achieve stable HO$_2$/NO.

Overall, SOA formation from oxidation of camphene may be potentially larger in polluted environments (e.g., urban environments) than NO$_x$-free environments. This reveals a possible underestimation of SOA formed from oxidation of camphene and possibly other BVOC in current models by assuming similar SOA yield dependence. Chamber studies of other understudied BVOC are therefore important to evaluate and improve model predictions.

Data Availability

The experimental data is available upon request from the corresponding authors. The modeling data used in this paper can be downloaded online: https://github.com/jia-jiang/SAPRC_Camphene.

Supplement

The supplement related to this article is available online at:

Author Contributions

460 QL and JJ contributed equally to the study. QL performed chamber experiments, data analysis and led the first draft of the manuscript. JJ derived and implemented the camphene mechanism in SAPRC, conducted SAPRC model simulations and led discussions on the chemistry of camphene SOA formation. IS carried out GECKO-A model simulations. QL and JJ interpreted the results and wrote the manuscript with IS. QL, JJ, KB and DC finalized the final manuscript. All the listed authors contributed to the revisions of the manuscript. The project was supervised by KB 465 and DC.

Competing Interests

The authors declare that they have no conflict of interest.

Acknowledgements

Reference

Afreh, I. K., Aumont, B., Camredon, M., and Barsanti, K. C.: Using GECKO-A to derive mechanistic understanding of SOA formation from the ubiquitous but understudied camphene, Atmos. Chem. Phys. Discuss., 475 https://doi.org/10.5194/acp-2020-829, 2020.

Akagi, S. K., Yokelson, R. J., Burling, I. R., Meinardi, S., Simpson, I., Blake, D. R., McMeeking, G. R., Sullivan, A., Lee, T., Kreidenweis, S., Urbanski, S., Reardon, J., Griffith, D. W. T., Johnson, T. J., and Weise, D. R.: Measurements of reactive trace gases and variable O3 formation rates in some South Carolina biomass burning plumes, Atmos. Chem. Phys., https://doi.org/10.5194/acp-13-1141-2013, 2013.

480 Atkinson, R. and Arey, J.: Gas-phase tropospheric chemistry of biogenic volatile organic compounds: A review, Atmos. Environ., 37, 197–219, https://doi.org/10.1016/S1352-2310(03)00391-1, 2003.

Atkinson, R., Aschmann, S. M., and Arey, J.: Rate constants for the gas-phase reactions of OH and NO3 radicals and O3 with sabinene and camphene at 296±2 K, Atmos. Environ. Part A, Gen. Top., https://doi.org/10.1016/0960-1686(90)90144-C, 1990.

485 Aumont, B., Szopa, S., and Madronich, S.: Modelling the evolution of organic carbon during its gas-phase tropospheric oxidation: Development of an explicit model based on a self generating approach, Atmos. Chem. Phys., https://doi.org/10.5194/acp-5-2497-2005, 2005.

Aumont, B., Valorso, R., Mouchel-Vallon, C., Camredon, M., Lee-Taylor, J., and Madronich, S.: Modeling SOA formation from the oxidation of intermediate volatility n-alkanes, Atmos. Chem. Phys., 12, 7577–7589, 490 https://doi.org/10.5194/acp-12-7577-2012, 2012.

Baruah, S. D., Gour, N. K., Sarma, P. J., and Deka, R. C.: OH-initiated mechanistic pathways and kinetics of camphene and fate of product radical: a DFT approach, Environ. Sci. Pollut. Res., https://doi.org/10.1007/s11356-017-0646-2, 2018.

Benelli, G., Govindarajan, M., Rajeswary, M., Vaseeharan, B., Alyahya, S. A., Alharbi, N. S., Kadaikunnan, S.,
495   Khaled, J. M., and Maggi, F.: Insecticidal activity of camphene, zerumbone and α-humulene from Cheilocostus speciosus rhizome essential oil against the Old-World bollworm, Helicoverpa armigera, Ecotoxicol. Environ. Saf., 148, 781–786, https://doi.org/10.1016/j.ecoenv.2017.11.044, 2018.

Bianchi, F., Kurtén, T., Riva, M., Mohr, C., Rissanen, M. P., Roldin, P., Berndt, T., Crounse, J. D., Wennberg, P. O., Mentel, T. F., Wildt, J., Junninen, H., Jokinen, T., Kulmala, M., Worsnop, D. R., Thornton, J. A., Donahue, N.,
500   Kjaergaard, H. G., and Ehn, M.: Highly Oxygenated Organic Molecules (HOM) from Gas-Phase Autoxidation Involving   Peroxy   Radicals: A   Key   Contributor   to   Atmospheric   Aerosol, https://doi.org/10.1021/acs.chemrev.8b00395, 27 March 2019.

Camredon, M., Aumont, B., Lee-Taylor, J., and Madronich, S.: The SOA/VOC/NOx system: An explicit model of secondary organic aerosol formation, Atmos. Chem. Phys., https://doi.org/10.5194/acp-7-5599-2007, 2007.

505   Canagaratna, M. R., Jimenez, J. L., Kroll, J. H., Chen, Q., Kessler, S. H., Massoli, P., Hildebrandt Ruiz, L., Fortner, E., Williams, L. R., Wilson, K. R., Surratt, J. D., Donahue, N. M., Jayne, J. T., and Worsnop, D. R.: Elemental ratio measurements of organic compounds using aerosol mass spectrometry: Characterization, improved calibration, and implications, Atmos. Chem. Phys., 15, 253–272, https://doi.org/10.5194/acp-15-253-2015, 2015.

Carter, W. P. L.: A detailed mechanism for the gas-phase atmospheric reactions of organic compounds, Atmos.
510   Environ. Part A, Gen. Top., 24, 481–518, https://doi.org/10.1016/0960-1686(90)90005-8, 1990.

Carter, W. P. L.: Development of ozone reactivity scales for volatile organic compounds, J. Air Waste Manag. Assoc., 44, 881–899, https://doi.org/10.1080/1073161x.1994.10467290, 1994.

Carter, W. P. L.: Documentation of the SAPRC-99 Chemical Mechanism for VOC Reactivity Assessment, Report to the   California   Air   Resources   Board.   Available   at   http://cert.ucr.edu/~carter/absts.htm#saprc99   and
515   http://www.cert.ucr.edu/~carter/reactdat.htm., 2000.

Carter, W. P. L.: Development of a condensed SAPRC-07 chemical mechanism, Atmos. Environ., 44, 5336–5345, https://doi.org/10.1016/j.atmosenv.2010.01.024, 2010a.

Carter, W. P. L.: Development of the SAPRC-07 Chemical Mechanism and Updated Ozone Reactivity Scales, 2010b.

Carter, W. P. L.: Documentation of the SAPRC-18 Mechanism; Report to California Air Resources Board Contract
520   No. 11-761, May, 2020. [online] Available from: https://intra.engr.ucr.edu/~carter/SAPRC/18/, 2020a.

Carter, W. P. L.: Gateway to the SAPRC Mechanism Generation System: http://mechgen.cert.ucr.edu/, last access: 30 March 2021.

Carter, W. P. L.: Estimates and Assignments used in the SAPRC-18 Mechanism Generation System; Report to California Air Resources Board Contract No. 11-761. In preparation. When completed, will be available at
525   http://intra.engr.ucr.edu/~carter/SAPRC/18, 2020b.

Carter, W. P. L., Cocker, D. R., Fitz, D. R., Malkina, I. L., Bumiller, K., Sauer, C. G., Pisano, J. T., Bufalino, C., and Song, C.: A new environmental chamber for evaluation of gas-phase chemical mechanisms and secondary aerosol formation, Atmos. Environ., 39, 7768–7788, https://doi.org/10.1016/j.atmosenv.2005.08.040, 2005.

530   Clark, C. H., Kacarab, M., Nakao, S., Asa-Awuku, A., Sato, K., and Cocker, D. R.: Temperature Effects on Secondary Organic Aerosol (SOA) from the Dark Ozonolysis and Photo-Oxidation of Isoprene, Environ. Sci. Technol., 50, 5564–5571, https://doi.org/10.1021/acs.est.5b05524, 2016.

Cocker, D. R., Flagan, R. C., and Seinfeld, J. H.: State-of-the-art chamber facility for studying atmospheric aerosol chemistry, Environ. Sci. Technol., 35, 2594–2601, https://doi.org/10.1021/es0019169, 2001.

DeCarlo, P. F., Kimmel, J. R., Trimborn, A., Northway, M. J., Jayne, J. T., Aiken, A. C., Gonin, M., Fuhrer, K.,

535   Horvath, T., Docherty, K. S., Worsnop, D. R., and Jimenez, J. L.: Field-deployable, high-resolution, time-of-flight aerosol mass spectrometer, Anal. Chem., 78, 8281–8289, https://doi.org/10.1021/ac061249n, 2006.

Donahue, N. M., Robinson, A. L., Stanier, C. O., and Pandis, S. N.: Coupled partitioning, dilution, and chemical aging of semivolatile organics, Environ. Sci. Technol., 40, 2635–2643, https://doi.org/10.1021/es052297c, 2006.

Donahue, N. M., Robinson, A. L., and Pandis, S. N.: Atmospheric organic particulate matter: From smoke to

540   secondary organic aerosol, Atmos. Environ., 43, 94–106, https://doi.org/10.1016/j.atmosenv.2008.09.055, 2009.

Eddingsaas, N. C., Loza, C. L., Yee, L. D., Chan, M., Schilling, K. A., Chhabra, P. S., Seinfeld, J. H., and Wennberg, P. O.: α-pinene photooxidation under controlled chemical conditions-Part 2: SOA yield and composition in low- and high-NO x environments, Atmos. Chem. Phys., 12, 7413–7427, https://doi.org/10.5194/acp-12-7413-2012, 2012.

545   Fry, J. L., Draper, D. C., Barsanti, K. C., Smith, J. N., Ortega, J., Winkler, P. M., Lawler, M. J., Brown, S. S., Edwards, P. M., Cohen, R. C., and Lee, L.: Secondary Organic Aerosol Formation and Organic Nitrate Yield from NO 3 Oxidation of Biogenic Hydrocarbons Terms of Use CC-BY, Environ. Sci. Technol, 48, https://doi.org/10.1021/es502204x, 2014.

Gaona-Colmán, E., Blanco, M. B., Barnes, I., Wiesen, P., and Teruel, M. A.: OH- and O3-initiated atmospheric

550   degradation of camphene: temperature dependent rate coefficients, product yields and mechanisms, RSC Adv., 7, 2733–2744, https://doi.org/10.1039/c6ra26656h, 2017.

Geron, C., Rasmussen, R., Arnts, R. R., and Guenther, A.: A review and synthesis of monoterpene speciation from forests in the United States, Atmos. Environ., https://doi.org/10.1016/S1352-2310(99)00364-7, 2000.

Gilman, J. B., Lerner, B. M., Kuster, W. C., Goldan, P. D., Warneke, C., Veres, P. R., Roberts, J. M., De Gouw, J. A.,

555   Burling, I. R., and Yokelson, R. J.: Biomass burning emissions and potential air quality impacts of volatile organic compounds and other trace gases from fuels common in the US, Atmos. Chem. Phys., https://doi.org/10.5194/acp-15-13915-2015, 2015.

Griffin, R. J., Cocker, D. R., Flagan, R. C., and Seinfeld, J. H.: Organic aerosol formation from the oxidation of biogenic hydrocarbons, J. Geophys. Res. Atmos., https://doi.org/10.1029/1998JD100049, 1999.

560   Guenther, A.: A global model of natural volatile organic compound emissions, J. Geophys. Res., https://doi.org/10.1029/94JD02950, 1995.

Hakola, H., Arey, J., Aschmann, S. M., and Atkinson, R.: Product formation from the gas-phase reactions of OH radicals and O3 with a series of monoterpenes, J. Atmos. Chem., https://doi.org/10.1007/BF00694375, 1994.

Hatch, L. E., Luo, W., Pankow, J. F., Yokelson, R. J., Stockwell, C. E., and Barsanti, K. C.: Identification and quantification of gaseous organic compounds emitted from biomass burning using two-dimensional gas chromatography-time-of-flight mass spectrometry, Atmos. Chem. Phys., https://doi.org/10.5194/acp-15-1865-2015, 2015.

Hatch, L. E., Jen, C. N., Kreisberg, N. M., Selimovic, V., Yokelson, R. J., Stamatis, C., York, R. A., Foster, D., Stephens, S. L., Goldstein, A. H., and Barsanti, K. C.: Highly Speciated Measurements of Terpenoids Emitted from Laboratory and Mixed-Conifer Forest Prescribed Fires, Environ. Sci. Technol., https://doi.org/10.1021/acs.est.9b02612, 2019.

Hatfield, M. L. and Huff Hartz, K. E.: Secondary organic aerosol from biogenic volatile organic compound mixtures, Atmos. Environ., 45, 2211–2219, https://doi.org/10.1016/j.atmosenv.2011.01.065, 2011.

Hayward, S., Muncey, R. J., James, A. E., Halsall, C. J., and Hewitt, C. N.: Monoterpene emissions from soil in a Sitka spruce forest, Atmos. Environ., https://doi.org/10.1016/S1352-2310(01)00213-8, 2001.

Henze, D. K., Seinfeld, J. H., Ng, N. L., Kroll, J. H., Fu, T. M., Jacob, D. J., and Heald, C. L.: Global modeling of secondary organic aerosol formation from aromatic hydrocarbons: High- vs. low-yield pathways, Atmos. Chem. Phys., 8, 2405–2421, https://doi.org/10.5194/acp-8-2405-2008, 2008.

Hurley, M. D., Sokolov, O., and Wallington, T. J.: Organic aerosol formation during the atmospheric degradation of toluene, Environ. Sci. Technol., 35, 1358–1366, https://doi.org/10.1021/es0013733, 2001.

Jay R. Odum, Thorsten Hoffmann, Frank Bowman, Don Collins, Richard C. Flagan, and John H. Seinfeld: Gas/Particle Partitioning and Secondary Organic Aerosol Yields, 2580–2585 pp., https://doi.org/10.1021/ES950943, 1996.

Jiang, J., Carter, W. P. L., Cocker, D. R., and Barsanti, K. C.: Development and Evaluation of a Detailed Mechanism for Gas-Phase Atmospheric Reactions of Furans, ACS Earth Sp. Chem., 4, 1254–1268, https://doi.org/10.1021/acsearthspacechem.0c00058, 2020a.

Jiang, J., Carter, W. P. L., Cocker, D. R., and Barsanti, K. C.: Development and Evaluation of a Detailed Mechanism for Gas-Phase Atmospheric Reactions of Furans, ACS Earth Sp. Chem., 4, 1254–1268, https://doi.org/10.1021/acsearthspacechem.0c00058, 2020b.

Komenda, M.: Monoterpene emissions from Scots pine (Pinus sylvestris): Field studies of emission rate variabilities, J. Geophys. Res., 107, 4161, https://doi.org/10.1029/2001JD000691, 2002.

Kroll, J. H. and Seinfeld, J. H.: Chemistry of secondary organic aerosol: Formation and evolution of low-volatility organics in the atmosphere, https://doi.org/10.1016/j.atmosenv.2008.01.003, 1 May 2008.

Kroll, J. H., Ng, N. L., Murphy, S. M., Flagan, R. C., and Seinfeld, J. H.: Secondary organic aerosol formation from isoprene photooxidation, Environ. Sci. Technol., 40, 1869–1877, https://doi.org/10.1021/es0524301, 2006.

Kuwata, M., Zorn, S. R., and Martin, S. T.: Using elemental ratios to predict the density of organic material composed of carbon, hydrogen, and oxygen, Environ. Sci. Technol., 46, 787–794, https://doi.org/10.1021/es202525q, 2012.

Lannuque, V., Camredon, M., Couvidat, F., Hodzic, A., Valorso, R., Madronich, S., Bessagnet, B., and Aumont, B.:
600   Exploration of the influence of environmental conditions on secondary organic aerosol formation and organic
       species properties using explicit simulations: Development of the VBS-GECKO parameterization, Atmos. Chem.
       Phys., 18, 13411–13428, https://doi.org/10.5194/acp-18-13411-2018, 2018.

Li, L., Tang, P., and Cocker, D. R.: Instantaneous nitric oxide effect on secondary organic aerosol formation from m-
       xylene photooxidation, Atmos. Environ., 119, 144–155, https://doi.org/10.1016/j.atmosenv.2015.08.010, 2015.

Li, Q., Hu, D., Leungsakul, S., and Kamens, R. M.: Large outdoor chamber experiments and computer simulations:
605   (I) Secondary organic aerosol formation from the oxidation of a mixture of d-limonene and α-pinene, Atmos.
       Environ., 41, 9341–9352, https://doi.org/10.1016/j.atmosenv.2007.09.017, 2007.

Ludley, K. E., Jickells, S. M., Chamberlain, P. M., Whitaker, J., and Robinson, C. H.: Distribution of monoterpenes
       between organic resources in upper soil horizons under monocultures of Picea abies, Picea sitchensis and Pinus
       sylvestris, Soil Biol. Biochem., https://doi.org/10.1016/j.soilbio.2009.02.002, 2009.

610   Maleknia, S. D., Bell, T. L., and Adams, M. A.: PTR-MS analysis of reference and plant-emitted volatile organic
       compounds, Int. J. Mass Spectrom., https://doi.org/10.1016/j.ijms.2006.11.010, 2007.

Malloy, Q. G. J., Nakao, S., Qi, L., Austin, R., Stothers, C., Hagino, H., and Cocker, D. R.: Real-Time aerosol density
       determination utilizing a modified scanning mobility particle sizer aerosol particle mass analyzer system, Aerosol
       Sci. Technol., 43, 673–678, https://doi.org/10.1080/02786820902832960, 2009.

615   Mazza, G. and Cottrell, T.: Volatile components of roots, stems, leaves, and flowers of Echinacea species, J. Agric.
       Food Chem., https://doi.org/10.1021/jf981117y, 1999.

McVay, R. C., Zhang, X., Aumont, B., Valorso, R., Camredon, M., La, Y. S., Wennberg, P. O., and Seinfeld, J. H.:
       SOA formation from the photooxidation of α-pinene: Systematic exploration of the simulation of chamber data,
       Atmos. Chem. Phys., 16, 2785–2802, https://doi.org/10.5194/acp-16-2785-2016, 2016.

620   Mehra, A., Krechmer, J. E., Lambe, A., Sarkar, C., Williams, L., Khalaj, F., Guenther, A., Jayne, J., Coe, H., Worsnop,
       D., Faiola, C., and Canagaratna, M.: Oligomer and highly oxygenated organic molecule formation from oxidation
       of oxygenated monoterpenes emitted by California sage plants, Atmos. Chem. Phys., 20, 10953–10965,
       https://doi.org/10.5194/acp-20-10953-2020, 2020.

Moukhtar, S., Couret, C., Rouil, L., and Simon, V.: Biogenic Volatile Organic Compounds (BVOCs) emissions from
625   Abies alba in a French forest, Sci. Total Environ., 354, 232–245, https://doi.org/10.1016/j.scitotenv.2005.01.044,
       2006.

Mutzel, A., Rodigast, M., Iinuma, Y., Böge, O., and Herrmann, H.: Monoterpene SOA - Contribution of first-
       generation oxidation products to formation and chemical composition, Atmos. Environ., 130, 136–144,
       https://doi.org/10.1016/j.atmosenv.2015.10.080, 2016.

630   Nakao, S., Tang, P., Tang, X., Clark, C. H., Qi, L., Seo, E., Asa-Awuku, A., and Cocker, D.: Density and elemental
       ratios of secondary organic aerosol: Application of a density prediction method, Atmos. Environ., 68, 273–277,
       https://doi.org/10.1016/j.atmosenv.2012.11.006, 2013.

Nannoolal, Y., Rarey, J., and Ramjugernath, D.: Estimation of pure component properties part 3. Estimation of the vapor pressure of non-electrolyte organic compounds via group contribution and group interactions, Fluid Phase Equilib., 269, 117–133, https://doi.org/10.1016/j.fluid.2008.04.020, 2008.

Ng, N. L., Chhabra, P. S., Chan, A. W. H., Surratt, J. D., Kroll, J. H., Kwan, A. J., McCabe, D. C., Wennberg, P. O., Sorooshian, A., Murphy, S. M., Dalleska, N. F., Flagan, R. C., and Seinfeld, J. H.: Effect of NOx level on secondary organic aerosol (SOA) formation from the photooxidation of terpenes, Atmos. Chem. Phys., 7, 5159–5174, https://doi.org/10.5194/acp-7-5159-2007, 2007a.

Ng, N. L., Chhabra, P. S., Chan, A. W. H., Surratt, J. D., Kroll, J. H., Kwan, A. J., McCabe, D. C., Wennberg, P. O., Sorooshian, A., Murphy, S. M., Dalleska, N. F., Flagan, R. C., and Seinfeld, J. H.: Effect of NOx level on secondary organic aerosol (SOA) formation from the photooxidation of terpenes, Atmos. Chem. Phys., https://doi.org/10.5194/acp-7-5159-2007, 2007b.

Nøjgaard, J. K., Bilde, M., Stenby, C., Nielsen, O. J., and Wolkoff, P.: The effect of nitrogen dioxide on particle formation during ozonolysis of two abundant monoterpenes indoors, Atmos. Environ., 40, 1030–1042, https://doi.org/10.1016/j.atmosenv.2005.11.029, 2006.

Pankow, J. F.: An absorption model of the gas/aerosol partitioning involved in the formation of secondary organic aerosol, Atmos. Environ., 41, 75–79, https://doi.org/10.1016/j.atmosenv.2007.10.060, 1994.

Presto, A. A., Huff Hartz, K. E., and Donahue, N. M.: Secondary organic aerosol production from terpene ozonolysis. 2. Effect of NOx concentration, Environ. Sci. Technol., 39, 7046–7054, https://doi.org/10.1021/es050400s, 2005.

Pullinen, I., Schmitt, S., Kang, S., Sarrafzadeh, M., Schlag, P., Andres, S., Kleist, E., Mentel, T. F., Rohrer, F., Springer, M., Tillmann, R., Wildt, J., Wu, C., Zhao, D., Wahner, A., and Kiendler-Scharr, A.: Impact of NOxon secondary organic aerosol (SOA) formation from α-pinene and β-pinene photooxidation: The role of highly oxygenated organic nitrates, Atmos. Chem. Phys., 20, 10125–10147, https://doi.org/10.5194/acp-20-10125-2020, 2020.

Pye, H. O. T., Chan, A. W. H., Barkley, M. P., and Seinfeld, J. H.: Global modeling of organic aerosol: The importance of reactive nitrogen (NOx and NO3), Atmos. Chem. Phys., 10, 11261–11276, https://doi.org/10.5194/ACP-10-11261-2010, 2010.

Pye, H. O. T., D'Ambro, E. L., Lee, B. H., Schobesberger, S., Takeuchi, M., Zhao, Y., Lopez-Hilfiker, F., Liu, J., Shilling, J. E., Xing, J., Mathur, R., Middlebrook, A. M., Liao, J., Welti, A., Graus, M., Warneke, C., de Gouw, J. A., Holloway, J. S., Ryerson, T. B., Pollack, I. B., and Thornton, J. A.: Anthropogenic enhancements to production of highly oxygenated molecules from autoxidation, Proc. Natl. Acad. Sci. U. S. A., 116, 6641–6646, https://doi.org/10.1073/pnas.1810774116, 2019.

Sarrafzadeh, M., Wildt, J., Pullinen, I., Springer, M., Kleist, E., Tillmann, R., Schmitt, S. H., Wu, C., Mentel, T. F., Zhao, D., Hastie, D. R., and Kiendler-Scharr, A.: Impact of NOx and OH on secondary organic aerosol formation from β-pinene photooxidation, Atmos. Chem. Phys., 16, 11237–11248, https://doi.org/10.5194/acp-16-11237-2016, 2016.

Schervish, M. and Donahue, N. M.: Peroxy radical chemistry and the volatility basis set, Atmos. Chem. Phys., 20, 1183–1199, https://doi.org/10.5194/acp-20-1183-2020, 2020.

Song, C., Na, K., and Cocker, D. R.: Impact of the hydrocarbon to NOx ratio on secondary organic aerosol formation,
670 Environ. Sci. Technol., https://doi.org/10.1021/es0493244, 2005.

White, M. L., Russo, R. S., Zhou, Y., Mao, H., Varner, R. K., Ambrose, J., Veres, P., Wingenter, O. W., Haase, K.,
Stutz, J., Talbot, R., and Sive, B. C.: Volatile organic compounds in northern New England marine and continental
environments during the ICARTT 2004 campaign, J. Geophys. Res. Atmos.,
https://doi.org/10.1029/2007JD009161, 2008.

675 Zhang, S.-H., Shaw, M., Seinfeld, J. H., and Flagan, R. C.: Photochemical Aerosol Formation From c-Pinene-and 13-
Pinene, JOURNAL OF GEOPHYSICAL RESEARCH, 717–737 pp., 1992.

Zhao, Y., Thornton, J. A., and Pye, H. O. T.: Quantitative constraints on autoxidation and dimer formation from direct
probing of monoterpene-derived peroxy radical chemistry, Proc. Natl. Acad. Sci. U. S. A., 115, 12142–12147,
https://doi.org/10.1073/pnas.1812147115, 2018.

680 Ziemann, P. J. and Atkinson, R.: Kinetics, products, and mechanisms of secondary organic aerosol formation, Chem.
Soc. Rev., 41, 6582–6605, https://doi.org/10.1039/c2cs35122f, 2012.